In Situ Characterization of Colloidal Spheres by Synchrotron Small-Angle X-ray Scattering

ARTICLE *in* LANGMUIR · NOVEMBER 1997

Impact Factor: 4.46 · DOI: 10.1021/la970422v

4 AUTHORS:

Mischa Megens
Philips
54 PUBLICATIONS **1,858** CITATIONS
SEE PROFILE

Carlos van kats
Utrecht University
27 PUBLICATIONS **1,085** CITATIONS
SEE PROFILE

Peter Boesecke
European Synchrotron Radiation Facility
32 PUBLICATIONS **956** CITATIONS
SEE PROFILE

Willem L. Vos
University of Twente
223 PUBLICATIONS **6,636** CITATIONS
SEE PROFILE

In Situ Characterization of Colloidal Spheres by Synchrotron Small-Angle X-ray Scattering

Mischa Megens,[†] Carlos M. van Kats,[†,‡] Peter Bösecke,[§,||] and Willem L. Vos*[,†]

van der Waals-Zeeman Instituut, Universiteit van Amsterdam, NL-1018 XE Amsterdam, The Netherlands, and European Synchrotron Radiation Facility, BP 220, F-38043 Grenoble Cédex, France

Received April 24, 1997. In Final Form: September 8, 1997[⊗]

We have performed small-angle X-ray scattering with a synchrotron source on dilute suspensions of colloidal spheres of polystyrene latex, Stöber silica, and microemulsion-grown silica. Many interference fringes are observed of the monodisperse particles over a large range of scattering vectors and more than 5 orders of magnitude in intensity. We present a straightforward method to deduce the radii, the size polydispersity, and the interface thickness of the particles from a Porod plot of one and the same *in situ* measurement. The radii agree very well with static light-scattering data. The radii are larger than the electron microscopy data of dry spheres and smaller than the hydrodynamic radii from dynamic light-scattering data. The size polydispersities are smaller than those obtained by electron microscopy, which is well explained by the intrinsic random errors of electron microscopy. We find that nearly all the particles have a homogeneous internal density and a sharp interface with the suspending medium of less than 1 nm wide. In one case of a stepwise synthesized particle, we have discerned a dense core and a less-dense shell, without contrast matching with the suspending liquid. It is concluded that synchrotron small-angle X-ray scattering is a very powerful technique for the *in situ* study of colloidal systems.

I. Introduction

Suspensions of monodisperse colloidal particles offer many exciting scientific opportunities.[1−3] They are of interest in their own right, because of their mesoscopic dimensions (10 nm to 1 μm) and their unique type of interactions.[2] Furthermore, because their behavior can under some circumstances be considered analogous to that of microscopic atomic systems, colloidal systems permit us to study certain phenomena (crystallization, glass transition) at experimentally much more convenient time and length scales. Last but not least, colloids are promising systems from an applied point of view, especially in optics,[4,5] since their typical length scale is of the order of optical wavelengths. The possibility of creating a photonic band gap[6,7] is just one fascinating illustration of the appealing prospects of optically multiple-scattering colloidal crystals.[8−12] In all cases an accurate determination of the size and structure of colloidal particles is crucial when it comes to comparing theory and experiment. Therefore, we present in this paper a synchrotron small-angle X-ray scattering (synchrotron SAXS) study of colloidal particles that are widely used, namely polystyrene latex and two types of silica spheres. Although the use of X-ray scattering for characterizing colloids has been known already since the early 1950's,[13−18] it does not seem to have found widespread application, in spite of the fact that SAXS has several major advantages: it probes a wide range of length scales, it allows us to probe inside the particles, the method is *in situ*, and it does not suffer from multiple scattering. Moreover, knowledge of the scattering from individual particles is of critical importance for the interpretation of scattering from groups of particles, *e.g.* colloidal crystals (see Figure 1).[10,11]

A multitude of methods other than SAXS, such as light scattering, sedimentation, and microscopy, are used to determine the properties of small particles.[1,19] In static light scattering (SLS), the scattered intensity of visible light is measured. The resulting diffraction patterns are compared to a model to determine the particle size. A disadvantage of the method is the lack of structure in the scattering pattern for radii below about 120 nm. As a result, it is impossible to deduce information about the internal structure of the spheres. Another commonly used technique is dynamic light scattering (DLS),[20] which is based on measuring the Doppler shifts due to Brownian

* Author for correspondence. E-mail: wvos@phys.uva.nl.

[†] Universiteit van Amsterdam. wwweb: http://gopher.phys.uva.nl:70/0/fnsis/onderzoek/scm/scmhome.htm.

[‡] Present address: van't Hoff Laboratory for Physical and Colloid Chemistry, Debye Institute, Utrecht University, Padualaan 8, NL-3584 CH Utrecht, The Netherlands.

[§] European Synchrotron Radiation Facility.

[||] Present address: MPG/ASMB c/o DESY, Notkestrasse 85, D-22603 Hamburg, Germany.

[⊗] Abstract published in *Advance ACS Abstracts,* November 1, 1997.

(1) Hunter, R. J. *Foundations of Colloid Science*; Clarendon: Oxford, 1993.

(2) Pusey, P. N. In *Liquids, Freezing and Glass Transition*; Hansen, J. P., Levesque, D., Zinn-Justin, J., Eds.; North-Holland: Amsterdam, the Netherlands, 1991; p 763.

(3) Lekkerkerker, H. N. W. See ref 2, p 977.

(4) Asher, S. A. U.S. Patent Nos. 4,627,689 and 4,632,517.

(5) *Development and Applications of Materials Exhibiting Photonic Band Gaps*; Bowden, C. M., Dowling, J. P., Everitt, H. O., Eds.; special issue of *J. Opt. Soc. Am. B* **1993**, *10*, 280.

(6) Yablonovich, E. *Phys. Rev. Lett.* **1987**, *58*, 2059.

(7) John, S. *Phys. Rev. Lett.* **1987**, *58*, 2486.

(8) Vos, W. L.; Sprik, R.; van Blaaderen, A.; Imhof, A.; Lagendijk, A.; Wegdam, G. H. *Phys. Rev. B* **1996**, *53*, 16231. In *Photonic Band Gap Materials*; Soukoulis, C. M., Ed.; Kluwer: Dordrecht, The Netherlands, 1996; p 107.

(9) Vos, W. L.; Megens, M.; van Kats, C. M.; Bösecke, P. *J. Phys.: Condens. Matter* **1996**, *8*, 9503.

(10) Megens, M.; van Kats, C. M.; Bösecke, P.; Vos, W. L. *J. Appl. Crystallogr.*, in press.

(11) Vos, W. L.; Megens, M.; van Kats, C. M.; Bösecke, P. *Langmuir* **1997**, *13*, 6004.

(12) Tarhan, İ. İ.; Watson, G. H. *Phys. Rev. Lett.* **1996**, *76*, 315. In *Photonic Band Gap Materials*; Soukoulis, C. M., Eds.; Kluwer: Dordrecht, 1996; p 93.

(13) Yudowitch, K. L. *J. Appl. Phys.* **1951**, *22*, 214.

(14) Danielson, W. E.; Shenfil, L.; DuMond, J. W. M. *J. Appl. Phys.* **1952**, *23*, 860.

(15) Leonard, B. R.; Anderegg, J. W.; Kaesberg, P.; Beeman, W. W. *J. Appl. Phys.* **1952**, *23*, 152.

(16) Guinier, A.; Fournet, G. *Small-Angle Scattering of X-Rays*; Wiley: New York, 1955.

(17) Guinier, A. *X-Ray Diffraction in Crystals, Imperfect Crystals, and Amorphous Bodies*; Dover Publications: New York, 1994.

(18) Feigin, L. A.; Svergun, D. I. *Structure Analysis by Small-Angle X-Ray and Neutron Scattering*; Plenum: New York, 1987.

(19) Barth, H. G.; Sun, S.-T. *Anal. Chem.* **1993**, *65*, 55R.

S0743-7463(97)00422-8 CCC: $14.00

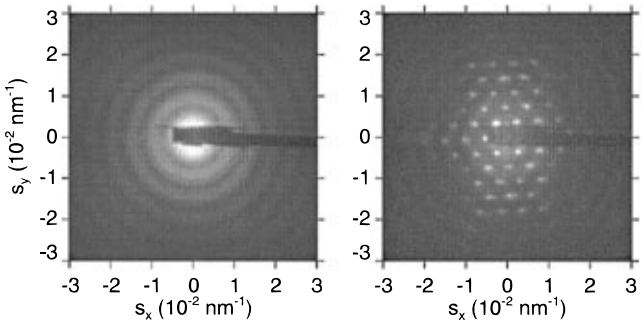

Figure 1. Diffraction patterns from a dilute suspension (left) and a colloidal crystal (right). The left pattern is for PS5020A polystyrene spheres (radius 102.0 nm) in ethanol, at a volume fraction of 0.1%. The right pattern is of a single crystal of the same particles, with fcc structure, 110 orientation, and 27 vol % density (see ref 11). The dark bar extending from the center to the right in both patterns is caused by the beam stop. The concentric rings in both patterns are a consequence of the form factor of the particles. The narrow peaks in the crystal diffraction pattern indicate that there is long-range order in the sample. Dividing the pattern from the crystal by the pattern from the suspension yields the structure factor F, in which the influence of particle shape has been eliminated.

motion of spheres in a liquid. Essentially one determines a diffusion constant, from which the radius can be obtained if the viscosity of the liquid and the shape of the particles are known.[21] Whether this is the true radius or a slightly larger 'hydrodynamic' radius depends on the presence of surfactants, salts, and the volume fraction of the colloid.[22] In addition to the radius, the size polydispersity can be determined from DLS measurements,[21−23] but by the nature of the method, DLS is not sensitive to the internal structure of the spheres. In sedimentation methods, one uses the fact that the sedimentation rate depends on the sphere size. The radius and polydispersity are determined directly from the sedimentation rate or from the density profile as a function of height. A different approach is to image individual spheres directly. This has the advantage that the size distribution is immediately obtained and that possibly coagulated particles can be detected. Optical microscopy is of course not suited for the purpose because the resolving power is insufficient for particles with a size on the order of a wavelength, but electron microscopy is appropriate. Unfortunately, for TEM one has to dry the samples and the spheres shrink in the process, by up to 10%.[24,25] Also the electrons sometimes degrade the material,[1,24] a phenomenon which is especially clear for polystyrene spheres, which seem to melt. Obviously these effects seriously hamper the accurate determination of sizes. A disadvantage of all methods mentioned is that they are not *in situ* techniques.

To probe inside the spheres, it is necessary to use a wavelength which is short compared to the size of the spheres. Scattering will then be predominantly in the forward direction: hence the designation 'small-angle scattering'.[16−18,26] Traditionally, colloidal systems are studied with small-angle neutron scattering (SANS),[27] whereas SAXS is much less used.[28] Nevertheless the potentials of SAXS have been demonstrated by Ballauff *et al.*[29−33] and in the use of ultrasmall-angle scattering by *e.g.* Dosho *et al.*[34] Surprisingly, hardly any use seems to have been made of synchrotron sources, except for the pioneering work of Sirota *et al.*[35] and Chang *et al.*[36] Modern synchrotron sources[18,37] have a high brilliance, so the acquisition time can be short (minutes); they deliver a highly monochromatic beam which is tightly collimated and has a narrow focus, so the angular resolution is high. In combination with the high dynamic range of the detector, this makes synchrotron SAXS an ideal tool for the study of colloidal systems. In the following sections we will demonstrate the strong capabilities of synchrotron SAXS regarding the characterization of nearly monodisperse colloidal spheres. We will compare SAXS radii with SLS, DLS, and TEM results, and we show that there is an especially simple way to determine small polydispersities using SAXS. In section II, we outline the experimental details, results are discussed in section III, and conclusions are drawn in section IV.

II. Experiment

Small-angle X-ray scattering measurements were done on beam line 4 (ID2) of the European Synchrotron Radiation Facility (ESRF) in Grenoble.[37] The X-ray beam is highly monochromatic ($\Delta\lambda/\lambda \approx 1.5 \times 10^{-4}$), is tightly collimated (beam divergence of about 30 μrad), and has a narrow focus (0.6 × 0.3 mm^2). The beamline is equipped with a two-dimensional gas-filled detector. Two-dimensional detection is invaluable when looking at anisotropic particles in external fields[38] or at the colloidal crystals that we are interested in[10,11] (see Figure 1). The two-dimensional detector of 18 cm diameter was positioned at the maximum distance of 10 m from the sample. Measurements were done in two runs, the first at a wavelength of $\lambda = 0.147\ 25$ nm and the second at $\lambda = 0.098\ 80$ nm, yielding a smallest accessible scattering vector $s = 2 \sin \theta/\lambda$ of approximately 3×10^6 or 5×10^6 m^{-1}, respectively, where 2θ is the scattering angle. The resolving power Δs is 5.5×10^5 or 7.5×10^5 m^{-1}, respectively. At the maximum sample−detector distance, the largest observable wave vector is over 8×10^7 m^{-1}.

Several different kinds of colloidal particles of various radii were used. Silica spheres were grown by Stöber synthesis[39] or by polymerization in a microemulsion[40,42] or were kindly provided by Alfons van Blaaderen[41,42] and Arnout Imhof.[43,44] Polystyrene

(20) Dynamic Light Scattering (DLS) is also known as photon correlation spectroscopy (PCS) or quasi-elastic light scattering (QELS).

(21) Berne, B.; Pecora, R. *Dynamic Light Scattering*; Wiley: New York, 1976.
(22) Duke, S. D.; Brown, R. E.; Layendecker, E. B. *Part. Sci. Technol.* **1989**, *7*, 223.
(23) Pusey, P. N.; van Megen, W. *J. Chem. Phys.* **1984**, *80*, 3513.
(24) van Helden, A. K.; Jansen, J. W.; Vrij, A. *J. Colloid Interface Sci.* **1981**, *81*, 354.
(25) Dobashi, T.; Yeh, F.; Ying, Q.; Ichikawa, K.; Chu, B. *Langmuir* **1995**, *11*, 4278.
(26) van der Hulst, H. C. *Light Scattering by Small Particles*; Dover Publications: New York, 1957.
(27) Ottewill, R. H. *J. Appl. Crystallogr.* **1991**, *24*, 436.
(28) Science Abstracts 1995 yields only 9 references when searched for the keywords "SAXS" and "colloid", while for "SANS" and "colloid" there are over 50 references.
(29) Grunder, R.; Kim, Y. S.; Ballauff, M.; Kranz, D.; Müller, H.-G. *Angew. Chem., Int. Ed. Engl.* **1991**, *30*, 1650.
(30) Grunder, R.; Urban, G.; Ballauff, M. *Colloid Polym. Sci.* **1993**, *271*, 563.
(31) Dingenouts, N.; Kim, Y. S.; Ballauff, M. *Colloid Polym. Sci.* **1994**, *272*, 1380.
(32) Ballauff, M.; Bolze, J.; Dingenouts, N.; Hickl, P.; Poetschke, D. *Macromol. Chem. Phys.* **1996**, *197*, 3043.
(33) Hickl, P.; Ballauff, M. *Physica A* **1997**, *235*, 238.
(34) Dosho, S.; Ise, N.; Ito, K.; Iwai, S.; Kitano, H.; Matsuoka, H.; Nakamura, H.; Okumura, H.; Ono, T.; Sogami, I. S.; Ueno, Y.; Yoshida, H.; Yoshiyama, T. *Langmuir* **1993**, *9*, 394.
(35) Sirota, E. B.; Ou-Yang, H. D.; Sinha, S. K.; Chaikin, P. M.; Axe, J. D.; Fujii, Y. *Phys. Rev. Lett.* **1989**, *62*, 1524.
(36) Chang, J.; Lesieur, P.; Delsanti, M.; Belloni, L.; Bonnet-Gonnet, C.; Cabane, B. *J. Phys. Chem.* **1995**, *99*, 15993.
(37) Bösecke, P.; Diat, O.; Rasmussen, B. *Rev. Sci. Instrum.* **1995**, *66*, 1636.
(38) Kroon, M.; Vos, W. L.; Wegdam, G. H. *Phys. Rev. E*, submitted.
(39) Stöber, W.; Fink, A.; Bohn, E. *J. Colloid Interface Sci.* **1968**, *26*, 62.
(40) Osseo-Asare, K.; Arriagada, F. J. *Colloid Surf.* **1990**, *50*, 321.
(41) van Blaaderen, A.; van Geest, J.; Vrij, A. *J. Colloid Interface Sci.* **1992**, *154*, 481.
(42) van Blaaderen, A.; Verhaegh, N. A. M.; Imhof, A.; Mason, N. In preparation).
(43) Imhof, A.; van Blaaderen, A.; Dhont, J. K. G. *Langmuir* **1994**, *10*, 3477.

colloids were obtained from Duke Scientific or kindly provided by Jan Verhoeven.[45] The particles were suspended in various solvents (water, methanol, ethanol, or dimethylformamide) by successively diluting and centrifuging. The final volume fraction of the diluted suspensions was usually 0.1% or less.

The colloidal suspensions were sealed in glass capillaries. For this purpose we employed 2 mm diameter round capillaries with 0.01 mm thin walls (Hilgenberg) and flat capillaries with a 0.3 or 0.4 mm inside path length and 0.3 mm thick walls (Vitro Dynamics). Because colloidal crystals usually have their close-packed planes parallel to the wall of the capillary, it is advantageous to use flat capillaries. Therefore we have also tried to measure diffraction patterns from dilute suspensions in the flat, thick-walled capillaries, but this resulted in a much higher background.[46] Most of the results discussed in section III were taken with thin-walled capillaries.

The raw diffraction pattern was corrected for the detector efficiency distribution which has been determined using the isotropic fluorescence radiation from a Sr-doped glass.[47] Absolute scattering intensities have been obtained by using a calibrated Lupolen polymer sample as a reference. We have obtained the differential scattering cross section per unit volume dI/dV by dividing the number of counts in a detector pixel by the number of incident photons, the solid angle subtended by the detector pixel, the transmission of the sample, and the thickness of the colloidal dispersion. Background intensities, caused by scattering from the capillary, from the window of the detector vacuum chamber, and from the beam stop, were determined by separate measurements on empty capillaries and subtracted.[48] The differential cross sections were azimuthally averaged to take full advantage of the acquired data. The typical integration time was 600s, which yields about 10^8 counts on the detector.

As an illustration, Figure 1 shows two measured diffraction patterns, one from a dilute suspension and another from a colloidal crystal of polystyrene spheres in methanol. The pattern from the dilute suspension (form factor F^2) consists of concentric rings, while the pattern from the crystal shows several narrow peaks (structure factor F [49]), multiplied by the same rings as in the pattern of the suspension. The narrow peaks in the structure factor indicate that there is long-range order in the sample over distances of several tenths of millimeters. The figure clearly shows the advantage of two-dimensional detection: the information about the azimuthal position of the peaks is obviously lost in the case of a lower dimensional detector. As will be explained below, the form factor provides valuable information about the size and internal structure (edge thickness, density gradients) of colloidal spheres, information that is difficult or impossible to obtain by other means, *e.g.* visible light scattering or electron microscopy. Moreover, form factor measurements are essential when studying colloidal crystals, since they enable us to extract structure factors from diffraction patterns of crystals.[10,11,27]

III. Results and Discussion

A. Particle Radii. Figure 2 shows the experimentally determined scattering cross section as a function of scattering vector s for dilute suspensions of the different kinds of particles studied: polystyrene, Stöber grown silica, and microemulsion-grown silica spheres. The cross sections vary over more than 5 orders of magnitude. The theoretical differential scattering cross section for a single homogeneous sphere with a sharp edge (i.e. the form factor) is[16−18]

$$I(s) = F^2(s) = I_e N_e{}^2 \Phi^2(2\pi sr) \qquad (1)$$

where $\Phi(x)$ is given in terms of the spherical Bessel

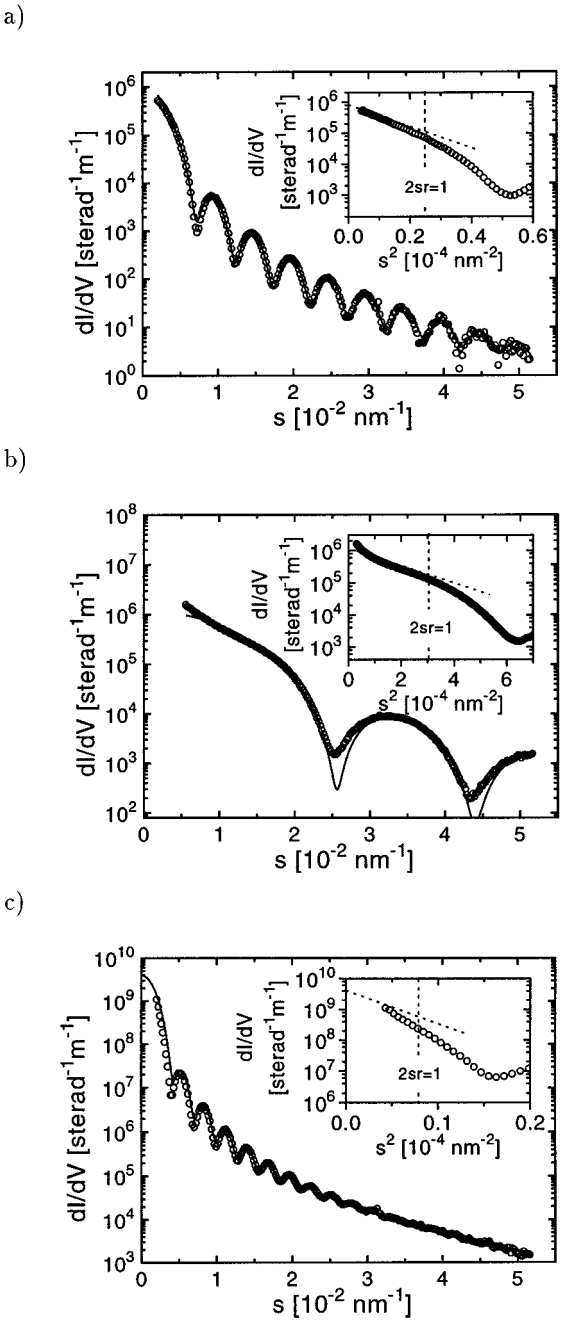

Figure 2. Differential scattering cross section dI/dV as a function of the scattering vector $s = 2\sin(\theta)/\lambda$ of dilute suspensions of spheres, plotted semilogarithmically (circles): (a) polystyrene in methanol (PS5020A); (b) microemulsion-grown silica in dimethylformamide (μEc1); (c) Stöber-grown silica in water (SC200). The presence of a large number of fringes indicates that the sizes of the spheres are highly monodisperse. The solid lines are model curves for spheres of homogeneous internal density. The inset shows the cross section as a function of s^2, at low s (Guinier-plot). The dashed lines with a slope of $(2\pi r)^2/5$ have been drawn using the radii deduced from the fringe period.

(44) Imhof, A.; van Blaaderen, A.; Maret, G.; Mellema, J.; Dhont, J. K. G. *J. Chem. Phys.* **1994**, *100*, 2170.

(45) Verhey, H. J.; Gebben, B.; Hofstraat, J. W.; Verhoeven, J. W. *J. Polym. Sci. A* **1995**, *33*, 339.

(46) The high background prevented an accurate determination of the polydispersity of the samples in the thick-walled capillaries. The background is especially bothersome at large s. As a result, the obtained scattering patterns are different from those obtained with thin-walled capillaries and do not decrease as s^{-4} but more slowly.

(47) Moy, J. P.; Hammersley, A. P.; Svensson, S. O.; Thompson, A.; Brown, K.; Claustre, L.; Gonzales, A.; McSweeney, S. *J. Synchrotron Radiat.* **1996**, *3*, 1.

(48) In the subtraction, the measured intensities were weighed by the transmission of the sample and the incident flux. To correct for the contributions from scattering by inhomogeneities inside the particles (fluctuation-induced scattering) and scattering by the suspending liquid, we adjusted the weighing factor slightly such that the final cross sections were positive for the measured range of s. Because the required changes in weighing factor are so small, this corresponds to subtracting a constant in the range of s where the subtraction has a significant influence.

(49) Hansen, J. P.; McDonald, I. R. *Theory of Simple Liquids*; Acadamic Press: London, 1986.

function j_1

$$\Phi(x) = 3j_1(x) = 3\frac{\sin(x) - x\cos(x)}{x^3} \qquad (2)$$

Here I_e is the differential cross section for forward scattering from a single electron (a constant), r is the radius of the sphere, $N_e = {}^4/_3\pi r^3 n_e$, and n_e is the excess electron density, *i.e.* the difference between the local electron density $n(\mathbf{r})$ and the average electron density of the sample. The interference of contributions from different parts of the particle gives rise to fringes in the scattering cross section as a function of s, that are clearly illustrated in Figure 2. The presence of a large number of fringes indicates that the spheres are nearly monodisperse, because even a moderate (~10%) size polydispersity (standard deviation of the radius divided by the mean) almost completely washes out the fringes. A common way to extract the radius and polydispersity[18,27,29−31,36,50] is to fit a model to the data, *i.e.* to minimize the deviations between the measured data and a calculated model curve in a least-squares sense, by varying the parameters of the model. However, more insight can be gained by presenting the data in a Porod plot (Figure 3), *i.e.* multiplied by s^4 and on a linear scale. For perfect spheres the resulting curves should go like $\cos(4\pi sr)$ at large sr (see eqs 1 and 2). The experimental curves indeed look like a cosine, but the oscillations gradually decrease with increasing s, as a consequence of the polydispersity of the spheres. The positions of the minima and maxima in the Porod plot are determined by the average sphere radius and hardly affected by a small polydispersity. Hence, the radius of the spheres can be very accurately determined by plotting the positions of the minima and maxima. The resulting plot for the polystyrene spheres is shown in Figure 4. The slope of the line corresponds to half the inverse radius. We have obtained a radius of the spheres in suspension of $r = 100.9 \pm 0.5$ nm, close to the radius specified by the manufacturer (Duke Scientific), $r = 99$ nm. The errors in the radii thus determined are on the order of only 0.5%, which clearly demonstrates the potential of the method.

We have obtained the radii for many dilute colloidal systems of nearly monodisperse spheres using synchrotron SAXS. The natures of the various systems, along with radii determined by other methods and the polydispersity, are summarized in Table 1. For some colloids we have measured the radius in several solvents. The radii were identical within experimental uncertainty,[51] which indicates that the spheres do not swell in the liquids that we have used.

A comparison between the results of SAXS and the other techniques, SLS, TEM, and DLS, is shown in Figure 5. We have plotted the ratios of the radii measured by the other techniques to the SAXS radii, as a function of SAXS radius. The radii determined by SAXS for the polystyrene systems are in excellent agreement with the radii specified by Duke Scientific. Furthermore, the radii obtained by SLS closely correspond to the SAXS radii, as expected because SLS and SAXS are basically the same techniques.[26] We take the excellent agreement as a validation of the SAXS technique. The relative error between SLS and SAXS radii is on the order of 3%, which is mainly due to the uncertainty in the SLS determination. Therefore the estimated uncertainties in the SLS radii are in agreement with the variation around the SAXS values

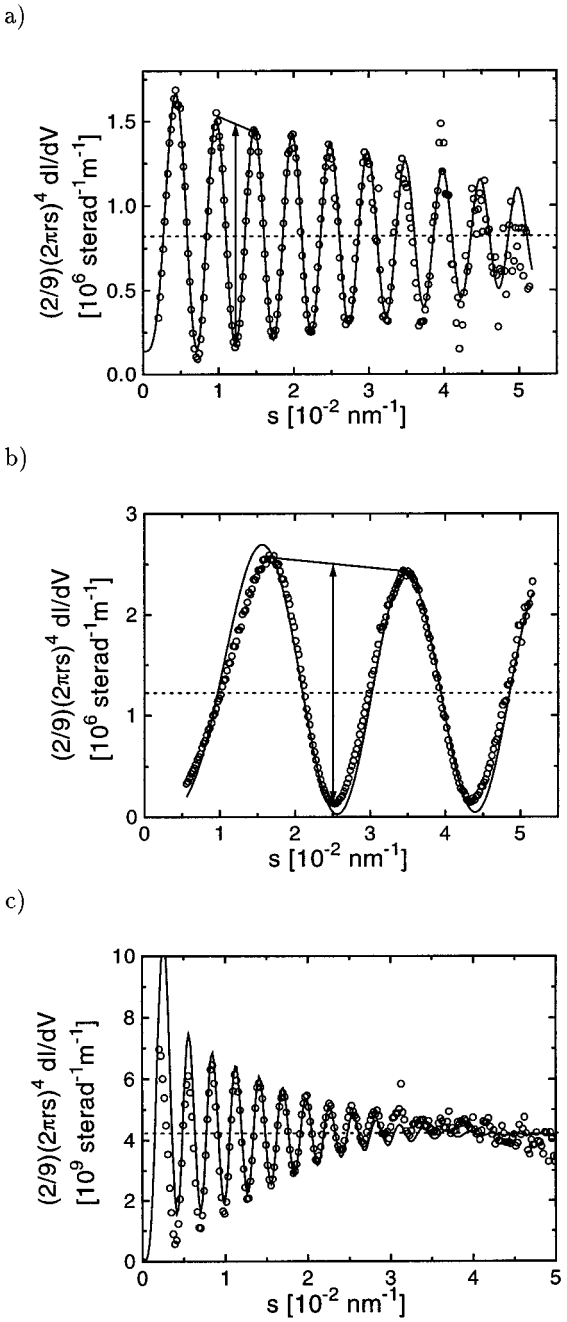

Figure 3. Differential scattering cross section dI/dV as a function of scattering vector $s = 2\sin(\theta)/\lambda$ (*cf.* Figure 2), plotted on a linear scale and multiplied by s^4 (Porod plot). (a) polystyrene in methanol (PS5020A); (b) microemulsion-grown silica in dimethylformamide (μEc1); (c) Stöber-grown silica in water (SC200). The polydispersity can be determined from the fringe amplitude (arrow) as a function of s. If the scattering cross section is multiplied by $(2/9)(2\pi sr)^4$ instead of s^4, then the average height of the fringes (dotted line) yields the cross section in the forward direction ($s = 0$), *cf.* inset in Figure 2. The solid lines are model curves for spheres of homogeneous internal density, taking into account size polydispersity and detector blurring.

shown in Figure 5, except for the SBE1/A6 system. The radii determined by TEM are systematically on the order of 10% lower than the SAXS and SLS results. This is probably because the spheres shrink when they are dried and bombarded with electrons in a TEM experiment. There is considerable variation in the TEM radii. One would expect that TEM radii can be determined with high accuracy, because it is possible to determine quite small polydispersities (down to a few percent) with TEM. The

(50) Pedersen, J. S. *J. Appl. Crystallogr.* **1994**, *27*, 595.

(51) One exception is the silica system SC200, which appears to be 3% larger in ethanol than in water or dimethylformamide. The radius of the SC200 system in ethanol was reproduced in two different runs. We have no explanation for this difference.

Table 1. Radii r (in Nanometers) and Polydispersities δ (in Percent) for a Number of Colloidal Systems, Obtained by Transmission Electron Microscopy (TEM), by Small-Angle Synchrotron X-ray Scattering (SAXS), by Static Light Scattering (SLS), by Dynamic Light Scattering (DLS), or from measurements by Duke Scientific (labeled "DS")[a]

system	r_{TEM}	r_{SAXS}	r_{SLS}	r_{DLS}	r_{DS}	δ_{TEM}	δ_{SAXS}
Thin-Walled Capillaries; Wavelength $\lambda = 0.147\ 25$ nm							
PS5020A		100.9 ± 0.5[b]			99	2.1[c]	2.3 ± 0.3
SC150[d]	114	145 ± 3[e]	148 ± 7	161			2
SC200	156	178.5 ± 0.7[e]	178 ± 5	216		3.6	3.05 ± 0.05
SC200		184 ± 0.4[f]					2.9 ± 0.1
SBE1/A6[l]	89.4	94.9 ± 1.6[g]	107.2 ± 0.3			6	5.5 ± 0.2
FSA7[m]	179	199.0 ± 1.8[g]	200 ± 3	188 ± 5		5.5	4.4 ± 0.3
SAF8[n]	187	211.4 ± 0.5[f]	211 ± 1	213 ± 3		4.0	2.4 ± 0.2
μESA9.3[o]		82.0 ± 0.4[h]	79.5				1.3 ± 0.1
μEc1	25.7	28.0 ± 0.5[h]				1.5	
μEc3		26.3 ± 0.5[h]					
Thick-Walled Capillaries; Wavelength $\lambda = 0.098\ 80$ nm							
PS5020A[i]		102.0 ± 0.3[j]			101.5	2.1[c]	
PS5022A		111.8 ± 0.3[f]			111	2.0[c]	
PS5024A		120.8 ± 0.5[f]			120.5	1.6[c]	
A11[p]	198.5[k]	200.6 ± 0.5		211.5			
SC150[d]	114	144 ± 2[f]	148 ± 7	161			
SC200	156	185.5 ± 1.3[f]	178 ± 5	216		3.6	
SC006	208	248.4 ± 1.1	241 ± 7	260			
μEc1	25.7	27.8 ± 0.4[h]				1.5	
μEc3		26.7 ± 0.5[h]					

[a] The TEM, SLS, and DLS measurements were done at the Van't Hoff Laboratory, Utrecht University. The colloidal systems have been split in three groups: first the polystyrene spheres, labeled "PS", then the Stöber grown silica systems, with an "S" in their name, and finally the microemulsion-grown silica systems, designated "μE". [b] In methanol. [c] Specified by Duke Scientific. [d] These spheres are not homogeneous but consist of a core of 101 ± 2 nm and shell of lower density of 37 ± 2 nm thickness. [e] In dimethylformamide or water. [f] In ethanol. [g] In water. [h] In dimethylformamide. [i] This dispersion is a different batch than the PS5020A at the other wavelength. [j] In methanol or ethanol. [k] SEM instead of TEM. [l] Reference 41. [m] Reference 43. [n] Reference 44. [o] Reference 42. [p] Reference 45.

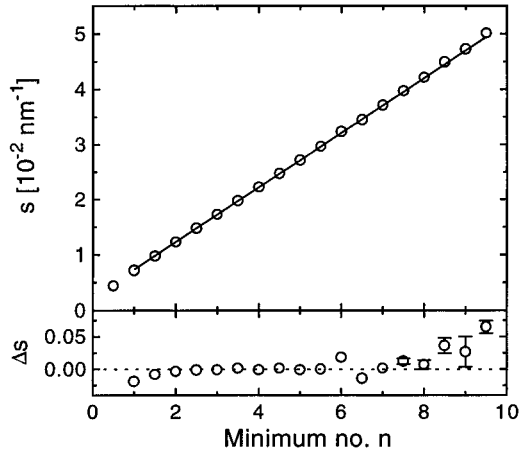

Figure 4. Positions of the minima and maxima in the Porod plot (PS5020A, Figure 3a) versus the order of the minimum (n) or maximum ($n + 1/2$). The slope of the fit (solid line) yields the radius, $r = 100.9 \pm 0.5$ nm, in excellent agreement with the value specified by the manufacturer (99 nm, Duke Scientific). The lower panel shows the small difference between the data points and the fit in the upper panel. Note that the simple straight line is not expected to accurately predict the position of the first maximum (leftmost data point).

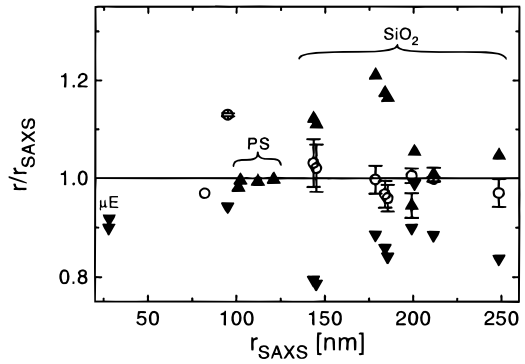

Figure 5. Ratios of the radii determined by dynamic light scattering (DLS, ▲), static light scattering (SLS, ○), and transmission electron microscopy (TEM, ▼) to the radii determined by SAXS, as a function of SAXS radius. The natures of the various colloidal systems are indicated. The SAXS radii are in good correspondence with those determined by SLS. The agreement with radii determined by Duke Scientific (polystyrene spheres, PS) is excellent. TEM radii are generally too small, and DLS radii too high.

variation suggests that different colloidal systems shrink by different amounts. The DLS radii tend to be higher than the radii determined by the other methods. This has been observed previously;[36] possibly the spheres drag some extra liquid along with them, for instance due to interactions with counterions which are in solution. Furthermore, there is a considerable variation in the DLS data, on the order of 10%. It has been shown previously that the DLS radius is rather sensitive to the presence of surfactants, salts, and the volume fraction of the colloid,[22] which may explain the variation in the DLS data. However, if one makes every effort, it is possible to determine very accurate radii using DLS.[23] This is clearly demonstrated by the excellent agreement between SAXS radii and the results of Duke Scientific (particles labeled "PS" in Figure 5), which were obtained by DLS.

B. Size Polydispersity. For perfectly monodisperse spheres, the curves in Figure 3 should go like $1 + \cos(4\pi sr)$ at large sr, but the amplitude of the modulations is slightly lower and decreases with increasing s. This is mainly a consequence of the polydispersity of the spheres: the form factors of spheres with different radii are identical, but the horizontal scale is different. The scattered intensities of individual spheres add, but with the fringes shifted, so the fringes average out. The fringes at high s are shifted more (in the absolute sense), so they average out more easily. Thus the decrease of the fringe amplitude is a measure of the polydispersity.

In a dilute suspension of non-interacting particles, the scattered intensity is the sum of intensities scattered by the individual particles, so the form factor should be averaged over the distribution of radii $D(r)$; *i.e.*, $I(s) = \int dr$

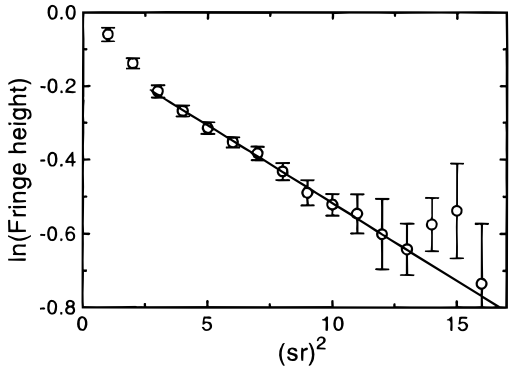

Figure 6. Amplitude of the fringes of PS5020A in Figure 3a, normalized to the average height, as a function of $(sr)^2$. The fringe amplitude decreases as $\exp(-2(2\pi sr\delta)^2)$ (except at low s, as expected), which is a straight line in this plot. The slope of the fit (solid line) yields the polydispersity, $\delta = 2.3 \pm 0.3\%$, in excellent agreement with the polydispersity specified by the manufacturer (2.1%, Duke Scientific).

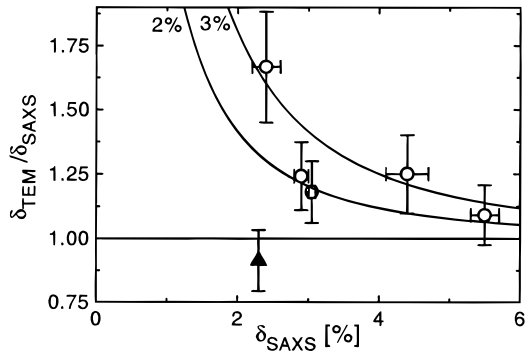

Figure 7. Ratios of the polydispersities determined by transmission electron microscopy (TEM, ○) or dynamic light scattering (DLS, Duke Scientific, ▲) to the polydispersities determined by SAXS, as a function of SAXS polydispersity. The DLS polydispersity specified by Duke Scientific and the polydispersity determined by SAXS are in excellent agreement. The TEM polydispersities are consistently higher, which is probably due to the random error in the determination of the radius of each individual sphere. The two curves indicate the expected overestimation of the TEM polydispersity in the case of 2% or 3% random error in the determination of TEM radii.

$I(s,r)\,D(r)$. A number of distributions have been proposed, for example the log−normal distribution, the Schulz distribution,[23,52] and the k-th order logarithmic distributions.[53] If the polydispersity is small however, these distributions all closely resemble a Gaussian distribution. For a Gaussian distribution, the average cross section can be calculated analytically. If we assume that the electron density n is the same for all spheres, it appears that the oscillating terms in Φ^2 decrease with a factor $\exp(-2(2\pi sr\delta)^2)$, where δ is the polydispersity, *i.e.* the standard deviation of the radius divided by the mean. This is a very useful result, because it provides a straightforward method to determine the polydispersity from the amplitudes of the fringes in a Porod plot, as we will demonstrate below shortly. Previously, it has been tried to determine the polydispersity from logarithmic plots of the scattering cross section; it is well-known that size polydispersity affects the depth of the minima in such plots.[17] The method that we present here involves a Porod plot instead. To our knowledge, this method for determining polydispersity has not been noticed before, in spite of the fact that it is both quantitative and convenient.

In Figure 6 we have plotted the amplitude of the fringes in Figure 3a (polystyrene spheres) as a function of $(sr)^2$. Such a semilogarithmic plot should give a straight line, except at low s, near the first maximum in the Porod plot.[54] Indeed the fringe amplitudes in Figure 6 agree with a straight line. From the slope of the line we find a polydispersity $\delta = \Delta r/r = 2.3 \pm 0.3\%$, which is in excellent agreement with the polydispersity specified by Duke Scientific, $\delta = 2.1\%$. It shows that SAXS is well suited to accurately determine small polydispersities (below 5%) that can now be routinely reached with refined particle synthesis methods.

There are several experimental effects which may also affect the amplitude of the fringes in Figure 3, namely the polychromaticity of the X-rays, the finite focus spot size, the beam divergence, and the finite detector resolution. Only one imperfection has the same influence as a polydispersity of the spheres: the deviation from monochromaticity of the X-rays. Fortunately, the relative spectral width of the source is approximately 1.5×10^{-4}, which is completely negligible compared to the polydispersities of colloidal dispersions ($> 10^{-2}$). For comparison, in small-angle neutron scattering (SANS) the relative spectral width is often of the order of 0.1; hence, this completely dominates the polydispersity of the spheres. The other effects, *i.e.* the focus size at the sample, the beam divergence, and the finite detector resolution, all affect the fringes in a similar way: the measured diffraction pattern is equal to the ideal pattern, convoluted with the profile of the direct beam. This convolution corresponds to small shifts of the diffraction pattern; because all fringes shift by equal amounts, they are all affected equally. It appears that due to these effects the fringe amplitude decreases by a factor which is independent of s. Thus it is possible to separate the influence of polydispersity and the instrument response, because the dependences on s of the effects are different. The abscissa of the line in Figure 6 is a measure of the width Δ of the beam profile. We find $\Delta = 0.72 \pm 0.10$ mm (r.m.s. width of a Gaussian beam profile). This is in reasonable agreement with the experimentally determined width of the direct beam on the detector, which is $\Delta = 0.60$ mm (horizontally) and 0.38 mm (vertically).

The polydispersities for several dilute colloidal systems of nearly monodisperse spheres have been determined using SAXS (see Table 1). The ratio of DLS or TEM polydispersities to SAXS polydispersities as a function of the SAXS polydispersity is plotted in Figure 7. Our data are in excellent agreement with the DLS data point obtained by Duke Scientific. This again confirms the validity of the SAXS technique. The error bars of the TEM ratios are based on the estimated error in the SAXS polydispersities and a relative error in the TEM polydispersities of 10%.[55] The TEM polydispersities are consistently larger than the corresponding SAXS polydispersities. The discrepancy gradually becomes larger with decreasing polydispersity. This can be explained from the method to determine polydispersities by TEM. TEM polydispersities are determined by measuring the diameters of a large number of particles on a grid and calculating the variance. The polydispersity is then computed as the root of the variance (*i.e.* the standard deviation) divided by the mean diameter. However, the

(52) Zimm, B. H. *J. Chem. Phys.* **1948**, *16*, 1093.
(53) Espenscheid, W. F.; Kerker, M.; Matijević, E. *J. Phys. Chem.* **1964**, *68*, 3093.
(54) The first fringe is expected to be a little bit higher, because the first fringe in a Porod plot of the form factor of a perfect sphere is also higher than the other fringes.
(55) The theoretical relative error in a TEM polydispersity is $1/(2k - 2)^{1/2}$, where k is the number of particle diameters measured; for $k = 50$ the relative uncertainty is ≈10%. The situation improves only slowly with particle number.

variance of the measured diameters is not equal to the variance of the distribution of diameters but also includes an additional contribution due to the random error in the determination of the diameters of the individual spheres. Because the magnification of the microscope is usually adjusted according to the size of the particles, one would expect the absolute error to be proportional to the particle size. The resulting measured TEM polydispersity is then $\delta_{TEM} = (\delta_{true}^2 + \delta_{err}^2)^{1/2}$, where δ_{true} is the true polydispersity of the particles and δ_{err} is the uncertainty in a measurement divided by the particle size. We have calculated this δ_{TEM} assuming that the SAXS polydispersity is correct and for a relative random error δ_{err} in the TEM radii of 2 and 3%. The resulting TEM/SAXS polydispersity ratios are plotted in Figure 7. The agreement with the experimentally observed ratio is striking. Hence we conclude that the small polydispersities determined by TEM are probably too high; *i.e.*, they are rather an upper bound for the true polydispersity of the particles.

A subtlety of the determination of diameters by TEM is which length to take if the particles are not perfect spheres but for instance ellipsoids. There are several approaches to the problem: averaging the length of the long and short axes or gauging the width of a particle in a fixed direction. For SAXS, the form factor for an ellipsoid is identical to that of a sphere with an effective radius which varies between the smallest and largest radii of the ellipsoid depending on its orientation.[26] The effective diameter is the width of the ellipsoid in the direction of the scattering vector. Thus apparently the result for the "gauging" method for determining the TEM radii is similar to the effective radius of SAXS.

Because ellipsoids in a dilute suspension have no preferential orientation, the effective SAXS scattering cross section of an ellipsoid is similar to the cross section of a sphere averaged over a distribution of radii. This is equivalent to a polydispersity for perfectly round spheres, so a polydispersity determined by SAXS necessarily includes a possible contribution due to the ellipticity of the particles. The distribution of effective radii for randomly oriented ellipsoids with axes of length $2R$, $2R$, and $2\nu R$ is very asymmetric, but for axial ratios ν close to 1, numerical integration shows that the effective cross section is mainly determined by the second moment of the distribution. The effective polydispersity is approximately $\delta = 0.3|\nu - 1|$. The average effective radius (related to the first moment of the distribution) is the geometric average of the largest and smallest semiaxis, $(\nu + 1)R/2$. Thus we see that the result for the "averaging" method for determining TEM radii is also very similar to the radius determined by SAXS and that (provided that the orientation of the ellipsoids on a TEM grid is random and $\nu \approx 1$) the "averaging" and "gauging" methods are equivalent.

C. Particle-Medium Interface. Measuring the scattering cross section out to large scattering vector s, *i.e.* more than just one fringe, in principle yields information at small length scales. If the polydispersity δ is not too large (<10%), then it is possible to look at the details of the spheres on a scale of $r\delta$ and sometimes even smaller. Some details have a pronounced effect on the SAXS diffraction pattern, even if the deviation from a perfect sphere of homogeneous density is small, for instance the presence of a smooth edge instead of a sharp one. So far we have assumed that the particles have a sharp edge, *i.e.* that the electron density abruptly changes at the interface to the medium. A smooth interface reveals itself immediately in the scattering cross section, as can be readily shown using the convolution theorem. The electron density of a particle with a smooth interface region can be constructed mathematically as the convolution of the electron density of a particle with a sharp edge and a smooth function which describes the blurring at the edge. The corresponding scattering cross section is the cross section of the particle with a sharp edge multiplied by the (squared) Fourier transform of the blurring function. If we take a Gaussian with a small width for the blurring function, then the cross section is multiplied by a broad Gaussian, so it starts to decrease faster than s^{-4} at high s. In a Porod plot like Figure 3, spheres with a sharp edge would show a function which oscillates around a constant value, while the function would gradually decrease at high s if the edge were smooth. Note that the decrease affects the cross section as a whole, not just the oscillating terms as with polydispersity, so the effects of a smooth edge and polydispersity can be separated.

Since the Porod cross section in Figure 3 oscillates around a constant value, we conclude that the edges of these spheres are rather sharp. Considering the average Porod cross section of the polystyrene spheres to be constant to within $\epsilon = 10\%$ over the whole range of s in the figure, we estimate the width σ_s of the interface-blurring Gaussian in reciprocal space from $(\exp(-s^2/2\sigma_s^2))^2 = 1 - \epsilon$. Taking $s = 5 \times 10^{-2}$ nm^{-1}, the upper bound for the thickness of the edge (σ of the corresponding Gaussian in real space) is $1/(2\pi\sigma_s) = 1.0$ nm, so the density indeed changes abruptly at the edge of the polystyrene spheres. Similar values are obtained for Stöber-synthesized silica. For silica surfaces, the edge layer has been reported[56] to have a thickness of 1−2 nm, in agreement with our result.

D. Electron Density. The forward scattering cross section $I(s \rightarrow 0)$ is related to the difference in electron density of the medium and of the particles, n_e, and the size and number of spheres in the scattering volume.[18] We can estimate the volume fraction of spheres in the liquid from the cross section using

$$\varphi = \frac{3}{n_e^2 4\pi r^3} \frac{1\ \mathrm{d}I}{r_e^2 \mathrm{d}V} \qquad (3)$$

The electron densities can be estimated from the number of atomic masses per proton M/Z and the mass density ρ. The densities for relevant materials are listed in Table 2. The radius is determined with high accuracy from the positions of the minima and maxima in the Porod plot (Figure 3). However, it is difficult to measure the forward scattering cross section because of the presence of the unscattered beam.

To estimate the forward cross section, the experimental cross section is extrapolated to $s = 0$ using a Guinier plot (see Figure 2, insets). The slope of $(2\pi r/s)^2$ in the Guinier approximation is estimated by using the radii determined in section III.A., *cf.* Table 1. The inset of Figure 2a reveals

Table 2. Electron Densities *n* of Relevant Colloidal Materials and Suspending Liquids, Estimated from the Number of Atomic Masses per Proton *M/Z* and the Mass Density *ρ*

material	structure	M/Z (amu/e$^-$)	ρ (g/cm^3)	n (e$^-$/nm^3)
methanol	CH_3OH	1.78	0.81	272
ethanol	C_2H_5OH	1.77	0.79	267
dimethylformamide	C_3H_7NO	1.83	0.95	311
polystyrene latex	C_8H_8	1.86	1.00−1.05	322−338
water	H_2O	1.80	1.00	333
silica (colloidal)	SiO_2	2.00	1.9−2.0[a]	570−600

[a] References 39, 43, and 58.

(56) Vigil, G.; Xu, Z.; Steinberg, S.; Israelachvili, J. *J. Colloid Interface Sci.* **1994**, *165*, 367.

an excellent agreement between the data and the Guinier approximation. This also demonstrates that there are no saturation effects of the detector. Saturation effects usually occur near the beam stop and would reveal a decrease at small s and a deviation from the straight line. For the microemulsion-grown silica (Figure 2b) the Guinier slope is also in good agreement with the data, except for a small deviation at small s. This is possibly due to a small number of coagulated spheres ("dumbbells") that occur in microemulsion-grown dispersions[42] and that were detected by TEM. These composite particles are larger; hence, they give rise to scattering at low s. Furthermore the cross section of these particles is larger, proportional to the volume of the particle, which explains why a small number of them is detectable. In Figure 2c, the Guinier slope is in moderate agreement with the data. We have no explanation for the not so good agreement in Figure 2c in comparison with Figure 2a and b.

The forward scattering cross section can also be derived from the Porod plot, as a check. The 'average Porod cross section' (dotted line in the Porod plots, Figure 3) should correspond to the scattering cross section extrapolated to $s = 0$ in Figure 2. The data of Figure 2a give a forward scattering cross section of 8.2×10^5 sr^{-1} m^{-1}, in good agreement with the Guinier estimate of $(7.5 \pm 0.4) \times 10^5$ sr^{-1} m^{-1}. However, the calibration of the absolute intensities was probably incorrect during the first run, and this affects the measured cross sections. In a later run we have repeated our measurements on PS5020A, PS5022A, and PS5024A colloids in ethanol, paying due attention to the determination of absolute intensities. We have prepared suspensions with volume fractions of 0.1%. From the forward scattering cross section we derived a difference in electron density of polystyrene and ethanol of 66, 89, and 67 nm^{-3}, respectively, in excellent agreement with the expected value of (66 ± 8) nm^{-3} (*cf.* Table 2). This shows that absolute intensities can be measured accurately.

The scattering cross section of polystyrene−water systems is very low, because the electron density of the most common solvent, water, is very closely matched to that of polystyrene. The weak scattering of this ubiquitous colloidal system may well be a reason why there have been so few reports on SAXS and colloids. For PS5022A spheres in water we have determined the forward scattering cross section to be less than 1.5×10^3 sr^{-1} m^{-1} at a volume fraction φ of 0.1%, which corresponds to a difference in electron density of the polystyrene spheres and water of less than 2%. The associated mass density of the colloidal polystyrene is 1.03 ± 0.02 g cm^{-3}, in good agreement with the density quoted by Duke Scientific, 1.05 g cm^{-3}.

Knowing the cross section in the forward direction, the radius, and the polydispersity, it is possible to calculate the complete scattering cross section as a function of s. These theoretical cross sections are shown as solid lines in Figures 2 and 3. The width of the detector profile is taken into account. The agreement with the experimentally observed cross sections is very good, especially for the polystyrene system, where it extends over more than 5 orders of magnitude. Only for the microemulsion-grown silica are there some small discrepancies, possibly caused by the presence of "dumbbells". We conclude that the cross sections of both polystyrene and Stöber silica systems are completely consistent with those of homogeneous, nearly monodisperse spheres with a sharp edge. Such a comparison of experimental and theoretical cross sections is quite a severe test, as will be demonstrated in the next section.

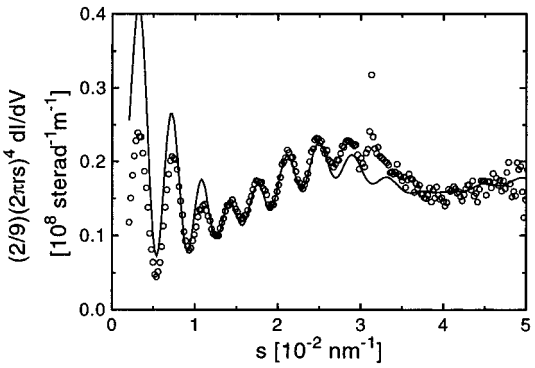

Figure 8. Porod plot of the differential scattering cross section dI/dV as a function of scattering vector s for a dilute suspension of SC150 silica spheres in water (circles). The minimum in the fringe amplitude around 1.5×10^{-2} nm^{-1} and the large wavelength modulation are likely caused by a core−shell structure. The solid line is a model of spheres with a homogeneous core (radius 107 nm) and a thin, less dense outer shell (thickness 37 nm). The model captures the essential features of the observed scattering cross section.

E. Internal Structure. An attractive capability of SAXS is the ability to examine the internal density of the spheres, *e.g.* to see whether the spheres consist of shells of different density. In such situations one traditionally resorts to neutron scattering while trying to match the scattering potential of one of the shells with that of the suspension liquid.[27] The technique of contrast matching can be applied to advantage with SAXS as well.[29−33] In fact, contrast matching is indispensable for detecting small density differences, as was demonstrated brilliantly in the experiments by Ballauff *et al.*[29−33] Here, we show that it is in some cases possible to detect inhomogeneities even without matching. This is probably feasible due to a considerable density difference.

As an illustration, the Porod cross section of a dilute suspension of silica spheres (SC150 in Table 1) is shown in Figure 8. These spheres have had no special treatment, but the cross section is totally different from the cross sections of the other spheres (*cf.* Figure 3). Similar silica systems (for instance SC200) give scattering patterns in accordance with that of homogeneous spheres, so there is something peculiar only with the SC150 system. As a check, we measured diffraction patterns for the same SC150 spheres in different liquids and at several different volume fractions, but the cross sections were identical.[57] The cross sections clearly show two oscillations corresponding to different length scales, a fast one corresponding to a sphere radius of about 95 nm and a slow one corresponding to 35 nm. An interesting feature of the scattering cross section in Figure 8 is that, at a wave vector s of about 1.5×10^{-2} nm^{-1}, the amplitude of the fringes has a minimum. Spheres consisting of a core and shell may show a minimum in the fringe amplitude as in Figure 8. Moreover, such a core-and-shell electron density is a reasonable assumption in view of the fact that silica spheres are often synthesized in steps, growing additional layers of silica on smaller particles until the desired diameter is reached. If the scattering cross section were a sum of several contributions, for instance if the sample were a mixture of two suspensions of nearly monodisperse spheres of different radii, then the amplitude of the fringes would decrease monotonously with increasing s.

The scattering cross section of a core-and-shell sphere can be easily calculated using the result for a homogeneous

(57) The small difference in electron density between the liquids used (DMF and water), as compared to the density of silica, does not cause significant changes in the shape of the scattering cross section.

sphere (eq 1 and 2): the excess electron density of the core-with-a-shell sphere can be made up of two homogeneous spheres, one having the radius of the core and the other having the outer radius. The scattering cross section is then

$$I(\text{core}-\text{shell}) = I_e N_e^2((1-\nu)\Phi(x) + \nu(1+b)^3\Phi(x(1+b)))^2 \quad (4)$$

where $x = 2\pi sr$ with r the radius of the core, d is the thickness of the shell, $b = d/r$ is the thickness of the shell as a fraction of the core radius, N_e is the number of excess electrons in the core, and ν is the electron density difference between the shell and the liquid as a fraction of the core excess electron density difference. Naturally, this cross section should be averaged over the distribution of core radii and shell thicknesses, and attention should be paid to the blurring due to the finite resolving power of the instrument. Instead of only one polydispersity, we now have three polydispersity parameters because variations in the core radius and shell thickness may be correlated. We chose to take two polydispersities, one for variations of the core radius and one for variations in the shell thickness, and a parameter c that accounts for a possible correlation, as follows:

$$\delta_r = \sqrt{\langle \Delta r^2 \rangle}/\langle r \rangle \quad (5)$$

$$\delta_d = \sqrt{\langle \Delta d^2 \rangle}/\langle d \rangle \quad (6)$$

$$c = \langle \Delta r \Delta d \rangle / \sqrt{\langle \Delta r^2 \rangle \langle \Delta d^2 \rangle} \quad (7)$$

where $\Delta r = r - \langle r \rangle$ and $\Delta d = d - \langle d \rangle$. The correlation coefficient c lies between -1 and $+1$. If $c = 0$, then the shell thickness is uncorrelated with the radius of the core. A fit to the core−shell model thus constructed (*i.e.* eq 4 averaged over a Gaussian distribution in r and d with polydispersities as indicated above) is shown in Figure 8. The fringe amplitude indeed has a minimum as a function of the scattering vector s. The calculated curve represents the observed scattering cross section reasonably well, although there are some discrepancies at small and large s. These may be caused by additional shells or density gradients in a sphere.

The calculated scattering cross section corresponds to spheres with a core radius r of 101 ± 2 nm and a shell thickness d of 37 ± 2 nm. Summing these values, one arrives at a total radius of 138 nm, slightly different from the value determined from the positions of the minima and maxima, 145 ± 3 nm, quoted in Table 1. The synthesis of the SC150 spheres was done in more than one step. Fortunately, the radius was measured before and after the last synthesis step. SLS measurements yielded radii of 101 ± 7 and 148 ± 7 nm, respectively, in good agreement with the radii of the core and shell determined from the SAXS data. From the SAXS data we can also determine the ratio of the core and shell excess electron densities. It appears that the electron density difference between the shell and the liquid is $\nu = 81 \pm 3\%$ of the excess electron density of the core. Using the electron densities of water and silica in Table 2, one estimates a mass density ratio of the shell and core of 92 ± 2%. This is a rather large difference in density, considering that the layers were grown using the same synthesis method. On the other hand, there is a comparable variation in the experimentally determined densities of colloidal silica.[24,39,43,58]

For the polydispersities of the core and shell of the curve shown in Figure 8 we have taken $\delta_r = 1.7\%$ and $\delta_d = 18\%$, but these values are not very accurate. The parameter c, that accounts for the correlation between variations of the core radius and variations of the shell thickness, was set at +1. The correlation coefficient c has to be definitely different from zero to reproduce the experimental results. If $c = 0$, then the observed typical modulation of the fringe amplitude is not reproduced. However, a model with $c = -1$ instead of +1 and a slightly different δ_d yields a very similar curve. This leads to the conclusion that the thickness of the shell is correlated to the size of the core; *i.e.*, the polydispersity of the spheres will change when a new layer is grown, but it is not possible to determine whether it will increase or decrease. A decrease in polydispersity is expected, on the basis of the growth mechanism.[41] The large value for δ_d in combination with the large correlation coefficient suggests that our model is probably a simplification of the true structure of the spheres. Nevertheless, our simple model demonstrates that it is in principle possible to detect with SAXS the influence of the size variation of the core particle on the thickness variation of a layer added in a next synthesis step.

IV. Conclusions

We have shown that the technique of synchrotron small-angle X-ray scattering (SAXS) is very well suited for the characterization of colloidal spheres. The size of colloidal spheres can be determined *in situ* and with high accuracy. We have determined the radii of many different kinds of colloidal spheres from the positions of the minima and maxima of the differential scattering cross section as a function of wave vector. The radii are in excellent agreement with those determined by SLS. TEM consistently yields radii that are smaller and DLS yields radii that are larger than the radii determined by synchrotron SAXS.

We have presented a straightforward method to deduce the size polydispersity of nearly monodisperse (polydispersity <10%) spheres from a Porod plot of the differential scattering cross section. A comparison with polydispersities determined by electron microscopy shows that the new method makes it possible to accurately determine even very small polydispersities (~2%). Moreover, our data suggest that TEM polydispersities are an upper bound to real polydispersities.

We have shown that it is possible to study the sharpness of the outer edge of the spheres. The thickness of the edge of polystyrene spheres of 100 nm radius was estimated to be less than 1 nm. Similar thicknesses are observed for silica spheres, in agreement with observations on silica surfaces. Thus, picturing polystyrene and silica spheres as objects with an abrupt edge is justified.

A Guinier plot was used to determine the forward scattering cross section, which in turn yields the volume fraction or the excess electron density of the spheres. The excess electron densities of several systems including the closely matched system polystyrene and water were obtained, in good agreement with literature data.

Using our data, we have calculated the scattering cross section as a function of wave vector, assuming that the spheres are homogeneous and that they have a sharp edge. The agreement of the calculated curves with the experimentally observed cross sections is excellent, especially

(58) Davis, K. E.; Russel, W. B.; Glantschnig, W. J. *J. Chem. Soc., Faraday Trans.* **1991**, *87*, 411.

for the polystyrene system where the agreement extends over 5 orders of magnitude.

As an example of a more complicated system, we have discussed a suspension of silica spheres which show a peculiar modulation in the cross section, caused by an inhomogeneous intraparticle density. The qualitative features of the cross section were captured by supposing that the spheres consist of a core surrounded by a shell of less dense material. This is a reasonable assumption because the spheres were synthesized by subsequent growth of silica layers. The core radius is in agreement with the size determined before the last synthesis step using static light scattering. The core radius, the shell thickness, and the ratio of the density of core and shell could be obtained even without contrast matching with the suspension liquid (*i.e., in situ*). The model indicates that the variations in core radius and shell thickness are correlated, as expected from the growth mechanism.

Acknowledgment. We would like to thank Alfons van Blaaderen, Arnout Imhof, and Jan Verhoeven for kindly providing some of the colloidal dispersions, and Alfons for useful and pleasant discussions. We thank Ad Lagendijk, Gerard Wegdam, and Rudolf Sprik for encouragements and support. The staff of the ESRF is thanked for assistance. This work is part of the research programme of the "Stichting voor Fundamenteel Onderzoek der Materie (FOM)", which is financially supported by the "Nederlandse Organisatie voor Wetenschappelijk Onderzoek (NWO)".

LA970422V